Inorganic Chemistry

pubs.acs.org/IC Article

Describing Polytopal Rearrangement Processes of Octacoordinate Structures. I. Renewed Insights into Fluxionality of the Rhenium Polyhydride Complex $ReH_5(PPh_3)_2$(Pyridine)

Yunwen Tao, Wenli Zou, Geng-Geng Luo, and Elfi Kraka*

Cite This: *Inorg. Chem.* 2021, 60, 2492−2502 Read Online

ACCESS | Metrics & More | Article Recommendations | Supporting Information

ABSTRACT: Hydride ligands of transition metal polyhydride complexes with a high coordination number are prone to fluxionality leading to interesting structural dynamics. However, the underlying polytopal rearrangement pathways have been rarely studied. Based on quantum chemical calculations carried out in this work with density functional theory and coupled-cluster theory, two new fluxional mechanisms have been identified for the rhenium polyhydride complex $ReH_5(PPh_3)_2$(pyridine) to jointly account for two consecutive coalescence events in the variable-temperature NMR spectra upon heating: lateral and basal three-arm turnstile rotation. The frequently cited pseudorotation in $ReH_5(PPh_3)_2$(pyridine) (Lee et al. *Inorg. Chem.* **1996,** *35,* 695) turns out to be a three-step process including two lateral three-arm turnstile steps and one basal turnstile step in between. The new fluxional mechanisms discovered in this work may also exist in other transition metal polyhydrides.

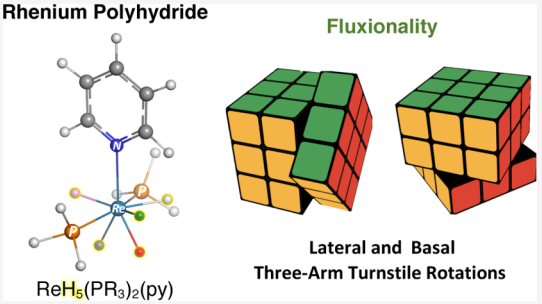

INTRODUCTION

The stereochemical nonrigidity of coordination compounds as an important structural property is realized via the dynamic processes termed polytopal rearrangement,[1,2] and it has recently been utilized in designing novel functional materials.[3] Representatives of this fluxionality include the well-known Berry pseudorotation in tetra-/pentavalent compounds,[4−6] the lever mechanism in SF_4,[7] the Muetterties' mechanisms in pentavalent compounds,[2,8] the chimeric pseudorotation in IF_5,[9] Bailar and Ray-Dutt twisting in hexacoordinate tris-chelate compounds,[10,11] and the Bartell mechanism in IF_7.[7,12] Dynamic NMR spectroscopy[13,14] (especially variable-temperature NMR) is a common technique to characterize the stereochemical nonrigidity in coordination compounds if the rate of the polytopal rearrangement is comparable to the NMR timescale.[15] In this case, the energy barriers of fluxional processes can be derived from the line shape analysis of NMR spectra,[16] but the NMR experiments are unable to disclose the exact mechanisms of fluxionality (i.e. how the atomic nuclei move during the polytopal rearrangement). Therefore, one has to employ quantum chemical calculations to explore all possible pathways of the fluxional process being investigated and then check whether the corresponding calculated energy barriers are reasonable.[17] Many theoretical studies have been reported to unravel the mechanistic details of the aforementioned polytopal rearrangement processes over the past two decades.[9,18−22]

As a part of our enduring interest in describing the polytopal rearrangement mechanisms with theoretical chemistry,[23] we chose the octacoordinate rhenium polyhydride complexes $ReH_5(PPh_3)_2L$ (L = pyridine and 2-(acetylamino)pyridine) as the subject to be investigated in this work. We chose rhenium polyhydrides as the first target in this series of investigations over other octacoordinate compounds[24−26] because fluxionality in rhenium polyhydrides is a current topic of interest in the experimental organometallic community.[27−29]

Rhenium polyhydrides are transition-metal hydrides with more than three hydrides bonded to the central rhenium atom.[30] These complexes are useful in organometallic chemistry for C−H bond activation,[31−35] and they can undergo substitution reactions where the coordinated H_2 is replaced by a two-electron donor.[30] Furthermore, rhenium polyhydrides have functioned as critical model systems in the conceptualization of dihydrogen bonds.[36−38]

The $ReH_5(PPh_3)_2$(pyridine) complex was first synthesized by Chatt and Coffey in 1969.[39] It features an octacoordinate dodecahedral structure as shown in Figure 1. Unlike most transition-metal polyhydride complexes with high coordination numbers being nonrigid even at the lowest attainable temperature, $ReH_5(PPh_3)_2$(pyridine) and its derivatives along with other rhenium polyhydrides[27,29,40−42] have shown high

Received: November 19, 2020
Published: February 3, 2021

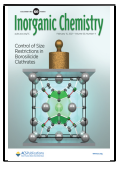

https://dx.doi.org/10.1021/acs.inorgchem.0c03418
Inorg. Chem. 2021, 60, 2492−2502

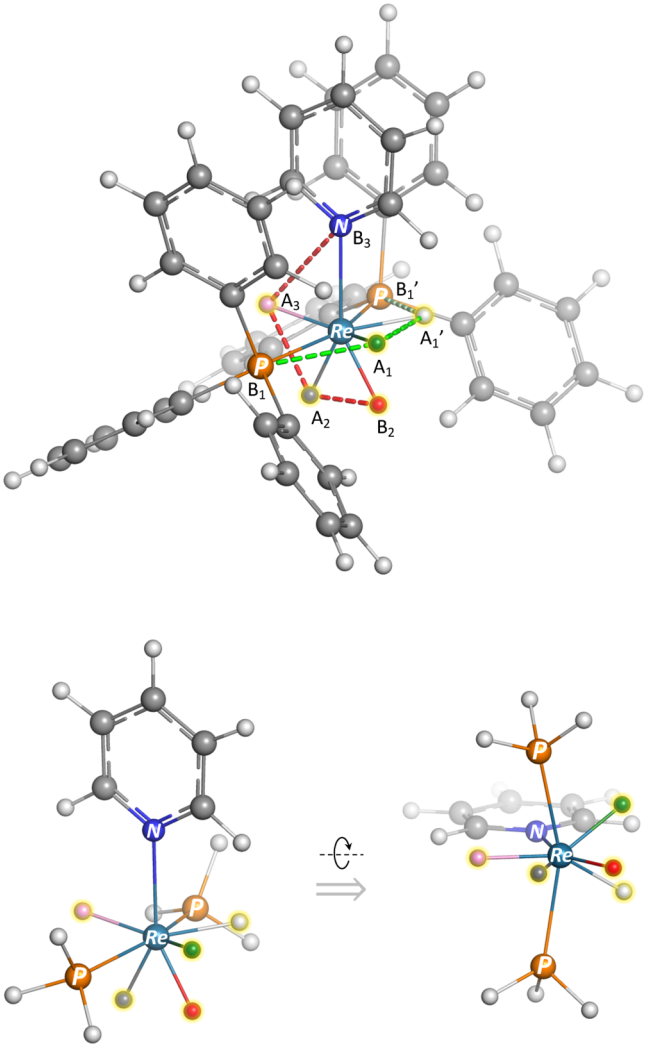

Figure 1. Ball-and-stick representation of the $ReH_5(PPh_3)_2$(pyridine) structure (top panel) and its simplified structure $ReH_5(PH_3)_2$(pyridine) omitting the phenyl groups (bottom panel) in order to reduce the computational cost of theoretical calculations. The five hydrides bonded to the central rhenium atom are highlighted with yellow color, and they are colored in white, green, red, gray, and pink. The red and green dashed lines as two orthogonal trapezoids in the complete $ReH_5(PPh_3)_2$(pyridine) structure are shown to illustrate the dodecahedral geometry. A and B sites are labeled with a black text while symmetry-equivalent sites are denoted with prime symbols. The simplified structure $ReH_5(PH_3)_2$(pyridine) is shown with two different perspectives.

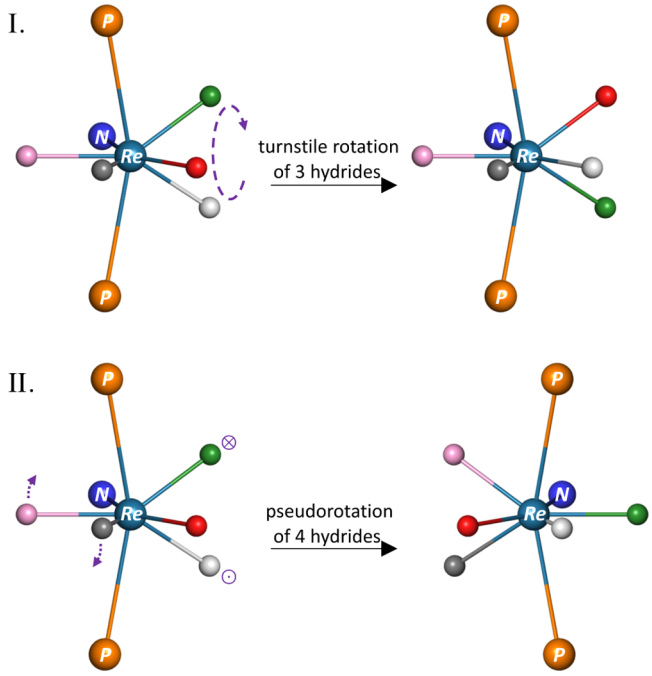

Figure 2. Two fluxional mechanisms of $ReH_5(PPh_3)_2$(py) proposed by Crabtree and co-workers.[43] Mechanism I is a 120° turnstile rotation motion of three hydrides colored in red, green, and white. Mechanism II consists of two pairwise rotations including (a) the up-/down-ward movement of pink/gray hydride and (b) the green/white hydride moving into/out of the plane of the paper. Mechanism II also inverts the relative steric relationship between the pyridine ligand and two triphenylphosphine ligands, leading to the pseudorotation of the whole molecule, reproduced from Inorg. Chem. 1996, 35(3), 695−699. Copyright 1996 American Chemical Society.

conformational rigidity at low temperatures permitting the ^{1}H NMR characterization of their fluxionality. In 1996, Crabtree, Rüegger, and co-workers observed two consecutive coalescence events in the variable-temperature NMR spectra of $ReH_5(PPh_3)_2$(pyridine) and proposed two fluxional mechanisms (see Figure 2) to account for this interesting coalescence behavior in the hydride region of the spectra.[43] In 1997, Crabtree, Eisenstein, and co-workers employed density functional theory (DFT) to verify one of the two abovementioned mechanisms (i.e. turnstile rotation) and discussed the influence on this mechanism from the Re−H···H−N dihydrogen bond caused by the ortho −NHAc group on the pyridine ligand.[44,45] However, to the best of our knowledge, there has been no theoretical investigation which is able to verify both the above two proposed fluxional mechanisms or to propose other alternative fluxional mechanisms concerning the five hydrides in $ReH_5(PPh_3)_2$(pyridine) and its derivatives since then.

In this work, we revisit the intricacies of fluxionality in $ReH_5(PPh_3)_2$(pyridine) and report two plausible fluxional mechanisms (i.e. lateral and basal three-arm turnstile rotations) that can jointly lead to the complete scrambling of all five hydrides based on the theoretical calculations with DFT and coupled-cluster theory. Although some recent NMR studies by Moehring and co-workers emphasized on (1) the rotational flexibility of the Re−N bond[27] and (2) the intermolecular exchange between one hydride ligand and a proton of the surrounding water molecule,[28] we believe that to fully understand the fluxionality concerning the five hydrides in $ReH_5(PPh_3)_2$(pyridine) (i.e. polytopal rearrangement) is an ideal starting point to solve the puzzles of fluxionality in rhenium polyhydrides.

This paper is structured in the following way. We first describe the details of the theoretical calculations conducted in this work in the Computational Details section. In the Results and Discussion section, we reassess the hydride assignment from the NMR spectroscopic results, present the mechanistic details of two three-arm turnstile rotations, and then examine the influence of the intramolecular Re−H···H−N dihydrogen bond on the above two turnstile processes. The conclusions are given in the last section.

https://dx.doi.org/10.1021/acs.inorgchem.0c03418
Inorg. Chem. 2021, 60, 2492−2502

COMPUTATIONAL DETAILS

Geometry optimization for local-minimum and transition-state structures of rhenium polyhydrides in this work was carried out with Truhlar's Minnesota pure functional M06-L[46] in combination with Ahlrichs' def2-SVP basis set.[47,48] Grimme's D3 empirical dispersion correction was added to the M06-L functional during geometry optimization.[49] Harmonic vibrational frequencies and corresponding thermodynamic corrections to the electronic energies were calculated at the same level of theory based on analytical second derivatives of the energy with regard to the Cartesian coordinates. Besides, the intrinsic reaction coordinate (IRC) calculations[50] were carried out starting from the optimized transition-state structures to trace out the reaction pathways of polytopal rearrangement processes. The NMR shielding tensors of five hydrides were calculated using the gauge-independent atomic orbital method at the M06-L/def2-TZVP level with or without the polarizable continuum model (PCM)[51] for implicit solvation by dichloromethane.

The single-point energies of the optimized structures were calculated at two different levels including (a) M06-L(D3)/def2-TZVP and (b) DLPNO-CCSD(T)/def2-TZVP. The domain-based local pair natural orbital coupled cluster (DLPNO-CCSD(T)) theory[52] with the resolution-of-identity (RI) technique was employed with "TightPNO" settings and the def2-TZVP/C auxiliary basis[53] using the ORCA 4.1.1 program.[54] All DFT calculations including single-point energies, geometry optimization, vibrational analysis, and IRC and NMR analysis were conducted with the Gaussian 16 package.[55]

The aforementioned high-level single-point electronic energies were added with the thermal corrections calculated at the M06-L(D3)/def2-SVP level (lower-level) in order to calculate the free energies at different temperatures.

RESULTS AND DISCUSSION

Re-evaluating Hydride Assignment from NMR Spectra. An important prerequisite for unraveling the mechanistic details of fluxionality in the rhenium polyhydride $ReH_5(PPh_3)_2$(pyridine) is that its variable-temperature NMR spectra are fully understood and correctly assigned because this is the basis for deducing the fluxional mechanisms.

When interpreting the NMR results at gradually increased temperatures, the low-temperature spectra with clearcut peaks before any coalescence or line broadening serve as the starting point. The rhenium polyhydride complex studied in this work has four well-separated peaks associated with the five hydrides at the low-temperature limit, and one peak has double intensity compared with the other three.[43] Given the dodecahedral geometry as the structural kernel, one can easily locate two plane-symmetric hydrides (green and white hydrides in Figure 3) contributing to the double intensity. For the remaining three hydrides, Crabtree and co-workers assigned their NMR peaks according to empirical rules.[43] Their assignment of ^{1}H NMR peaks to five hydrides was endorsed by the two-dimensional rotating-frame Overhauser effect spectroscopy (ROESY) which offers the information of proton pairs within 5 Å.[56] According to the measured ^{1}H ROESY spectrum, the pairwise distances among the remaining three hydrides (red, gray, and pink) are all below 5 Å. Furthermore, they observed that both the pink and green/white hydrides are within the 5 Å range with regard to the nearest protons at the ortho-positions

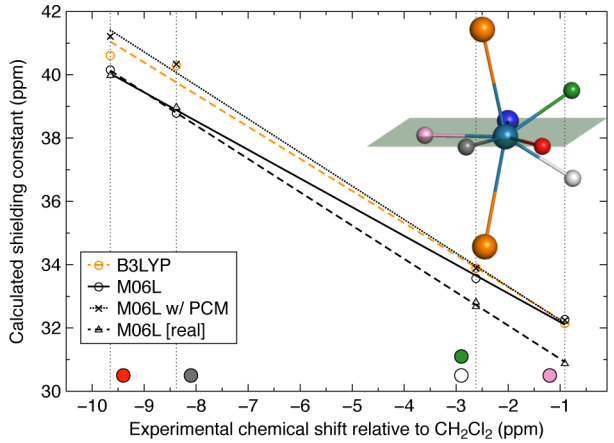

Figure 3. Comparison between calculated isotropic shielding constants at the DFT level with four different model chemistries and the experimentally measured ^{1}H chemical shifts for five hydrides in $ReH_5(PPh_3)_2$(pyridine). Four different model chemistries for NMR calculations are the following. **B3LYP**: Simplified structure in the gas phase at the B3LYP/def2-TZVP level; **M06L**: Simplified structure in the gas phase at the M06-L/def2-TZVP level; **M06L w/PCM**: Simplified structure with PCM of the dichloromethane solvent at the M06-L/def2-TZVP level; **M06L** [**real**]: Complete structure in the gas phase at the M06-L/def2-TZVP level. An ideal agreement between these two quantities is expected to have a linear fitting line with the slope being exactly −1, the coefficient of determination (R^2) being 1 and the root-mean-square error (RMSE) being 0. Detailed parameters of the four fitting lines are collected in Table 1. The pale−green plane is the mirror plane of the structure.

of the pyridine ligand. However, one needs to be aware of the fact that two protons having no signal shown in the ROESY spectrum are not necessarily distant from each other.[57] In this regard, the hydride assignment based on these measured NMR spectra is not utterly conclusive.

Therefore, we calculated the isotropic shielding constants of the five hydrides in the simplified structure $ReH_5(PH_3)_2$(pyridine) as well as the complete structure and then compared the calculated values against the experimentally measured ^{1}H chemical shifts of the five hydrides with respect to the dichloromethane peak. As shown in Figure 3, there exists a strong linear correlation between the calculated shielding constant values and the measured chemical shifts for the five hydrides. The shielding constants of hydrides can be converted into chemical shifts by subtracting from the ^{1}H shielding constants of dichloromethane; therefore, the fitting lines with their slopes close to −1 show that our calculations have unambiguously confirmed the previously reported hydride assignment[43] (see Figure 3) in a straightforward way.

A few technical aspects in modeling the NMR properties of the rhenium polyhydride complex need to be noted.

- The M06-L density functional[46] performs better than B3LYP[58] as the latter leads to slightly larger RMSE (see Table 1);
- Including the implicit solvation model and the phenyl groups attached to the phosphorus atoms does not help improve the linear correlation in Figure 3. In other words, the simplified structure $ReH_5(PH_3)_2$(pyridine) in the gas phase is already a satisfactory computational model for the purpose of hydride assignment.

Renewed Mechanistic Details of Fluxionality. Crabtree and co-workers proposed two possible fluxional mechanisms

https://dx.doi.org/10.1021/acs.inorgchem.0c03418
Inorg. Chem. 2021, 60, 2492−2502

Table 1. Parameters of the Four Fitting Lines in Figure 3 Including the Slope, Coefficient of Determination (R^2), and RMSE

model chemistry	slope	R^2	RMSE
B3LYP	−1.015	0.992	0.40
M06L	−0.907	0.999	0.15
M06L w/PCM	−1.059	0.998	0.21
M06L [real]	−1.053	0.999	0.15

(i.e. turnstile rotation and pseudorotation)[43] for the rhenium polyhydride $ReH_5(PPh_3)_2$(pyridine) as illustrated in Figure 2. In a subsequent study,[44] they carried out DFT calculations of the simplified structure $ReH_5(PH_3)_2$(pyridine) at the B3LYP/6-31G(d,p)/LANL2DZ level and located the transition state structure for the three-arm turnstile process which is associated with the first coalescence event in the variable-temperature ^{1}H NMR measurement upon heating. According to their calculations, the transition state structure is a result of 60° turnstile rotation of the triad of hydrides leading to a dodecahedral tautomer of the starting low-temperature structure. However, the transition state structure of the aforementioned pseudorotation mechanism was neither calculated nor explored in their investigation.

In this work, we reviewed the previous computational investigation,[44] conducted calculations on the simplified model $ReH_5(PH_3)_2$(pyridine) as well as its complete structure $ReH_5(PPh_3)_2$(pyridine) at the M06-L(D3)/def2-SVP level, and managed to identify two distinct three-arm turnstile rotation mechanisms (see Figure 4) that can satisfactorily interpret the coalescence events in the experimental variable-temperature NMR spectra and match the measured energy barriers from line shape analysis.

According to our calculations, the fluxionality of the studied rhenium polyhydride consists of two mutually dependent and similar mechanisms including (1) a lateral three-arm turnstile rotation and (2) a basal three-arm turnstile rotation. The stipulation of the lateral or basal position is based on the orientation of the rhenium polyhydride complex where the Re−N bond points upward while two Re−P bonds point to the front and back, respectively (see Figures 1 and 4).

The lateral three-arm turnstile rotation mechanism presented in this work closely resembles the first fluxional mechanism (i.e. turnstile rotation) proposed in the earlier work[43,44] but they are not exactly the same. As shown in Figure 4, the lateral turnstile rotation starts with the dodecahedral rhenium polyhydride structure at low temperatures (denoted

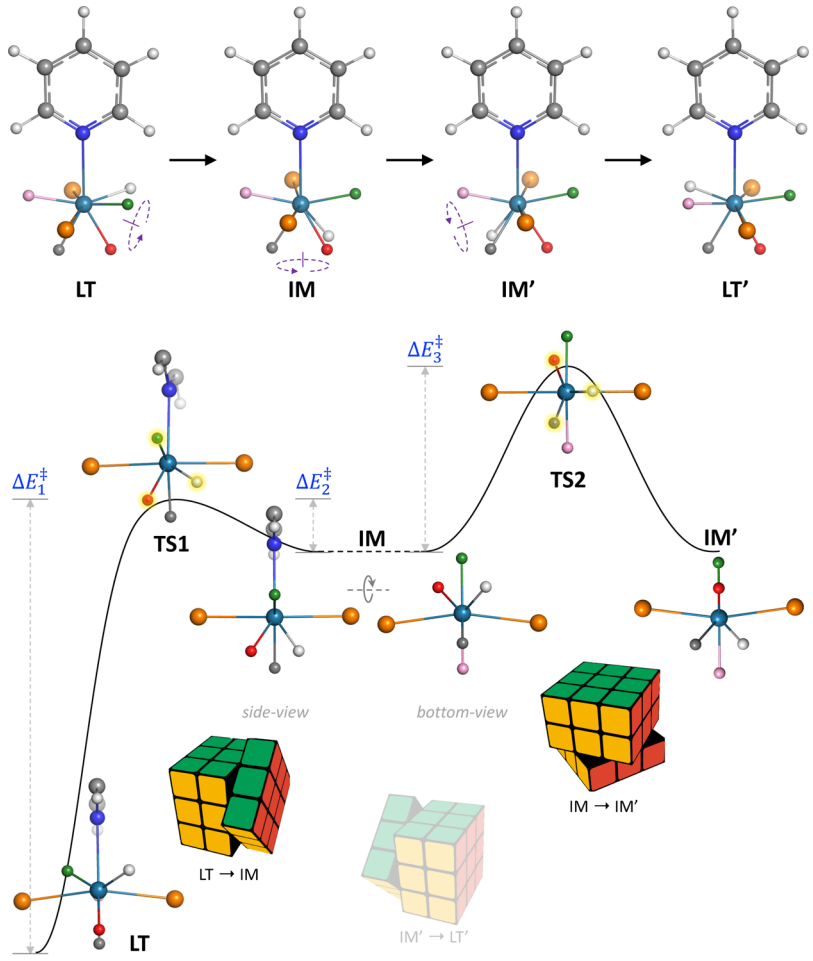

Figure 4. Representative polytopal rearrangement pathway (LT → IM → IM′ → LT′) for the $ReH_5(PPh_3)_2$(pyridine) structure leading to the complete scramble of five hydrides (top) and the energy profile of two elementary fluxional processes (bottom) including (a) lateral three-arm turnstile rotation LT → IM and (b) basal three-arm turnstile rotation IM → IM′. The color scheme for five hydrides is consistent with that in Figure 1. The hydrides within the two transition-state structures participating in the fluxional processes are highlighted with yellow color. The calculated activation barrier data ($\Delta E^{\ddagger}$) is collected in Table 2.

https://dx.doi.org/10.1021/acs.inorgchem.0c03418
Inorg. Chem. 2021, 60, 2492−2502

as **LT**) and the triad of hydrides on the right-hand side has the green and white hydrides above the red hydride. Due to the C_s symmetry in the complex, this triad of hydrides can rotate like a three-arm turnstile in two directions. For demonstration purpose, the clockwise direction was chosen where the green hydride goes up and the white hydride goes down. While the turnstile rotation proceeds by around 40° with the green hydride hanging above the white and red hydrides, the rhenium polyhydride structure reaches the first-order saddle point on the potential energy surface (with only one imaginary vibrational frequency) and this transition state denoted as **TS1** is about 10 kcal/mol higher in energy than **LT**. Noteworthy is that the **TS1** structure has a reduced symmetry (C_1). When this turnstile process continues by around 20°, it ends with an intermediate structure (**IM**) re-adopting the C_s symmetry with the mirror plane containing the pyridine ring. The **IM** structure as a dodecahedral tautomer of **LT** actually corresponds to the "transition state" structure obtained from the calculations by Crabtree and co-workers,[44] and the reason for this discrepancy may be that "the full Hessian was not computed" due to the limited computational capability back in 1997. The **IM** → **TS1** energy barrier is as low as 1 or 2 kcal/mol, and the geometric similarity between **IM** and **TS1** well exemplifies the Hammond–Leffler postulate.[59,60] With such a small energy barrier, **IM** can easily rotate the above-mentioned triad of hydrides anticlockwise back to **LT** or clockwise to an equivalent structure of **LT**, and this makes these three hydrides indistinguishable which could explain the first coalescence in NMR spectra.

The basal three-arm turnstile rotation mechanism requires that there are three hydrides trans to the pyridine ligand and in the bottom of the rhenium polyhydride complex. Therefore, it starts with the **IM** structure rather than **LT**. As shown in Figure 4, the three basal hydrides are colored in red, white, and gray, and this triad can also rotate like a turnstile in either direction. When this turnstile rotation proceeds clockwise by 30°, it arrives at the transition state structure **TS2** which is around 4 kcal/mol above **IM**. Noteworthy is that the **TS2** structure has also the C_s symmetry; however, its mirror plane is now perpendicular to the pyridine ring and contains two phosphorus atoms. With another 30° rotation, this basal turnstile process concludes with the intermediate structure **IM′** which is superposable on **IM**. Therefore, this basal three-arm turnstile rotation **IM** → **IM′** can be considered as a pseudorotation process of **IM**[1].[1] ([1]Note: This **IM**⇆**IM′** pseudorotation needs to be distinguished from the pseudorotation of **LT**.) With this basal turnstile mechanism, the three hydrides at the bottom also become indistinguishable given the rapid interconversion. While the energy of **TS2** is higher than **TS1**, both the lateral and basal turnstile mechanisms can coexist at higher temperatures, which makes all five hydrides indistinguishable accounting for the single broad NMR peak after the second coalescence event.

As illustrated in Figure 4, the **IM′** structure can have a lateral three-arm turnstile rotation for the triad of hydrides on the left-hand side as a reverse process of **LT** → **IM**, thus leading to the low-temperature structure **LT′** which is superposable on **LT**. We need to note that the **LT** → **IM** → **IM′** → **LT′** pathway actually leads to the pseudorotation of **LT**, which is closely related to the second mechanism (i.e. pseudorotation) proposed by Crabtree and co-workers (see Figure 2). However, our three-step pseudorotation consists of two lateral turnstile rotations and one basal turnstile rotation, and it is dissected in detail. By contrast, the pseudorotation mechanism proposed by Crabtree and co-workers[43] seems more complicated and cannot be verified with theoretical calculations.

We also checked whether the hybrid density functional B3LYP can lead to the same fluxional mechanisms which we have obtained in this work with Truhlar's M06-L functional because previous calculations[44] on this rhenium polyhydride system were carried out with the former density functional. According to our calculations, the B3LYP(D3)/def2-SVP level can reproduce the two transition state structures (**TS1** and **TS2**) obtained at the M06-L(D3)/def2-SVP level (see section S4 of Supporting Information). This means that the calculations based on the B3LYP functional will give the same lateral and basal three-arm turnstile mechanisms as discussed above.

To further justify the two fluxional mechanisms introduced in this work, we calculated single-point electronic and free energies of the structures involved in the two three-arm turnstile processes at the M06-L(D3)/def2-TZVP and DLPNO-CCSD(T)/def2-TZVP levels (see Table 2) to see if our calculated energy barriers match the free energy barriers derived from the measured NMR spectra.

Table 2. Calculated Electronic and Free Energy Barriers (in kcal/mol) of the Fluxional Processes in Figure 4′[a]

electronic		$\Delta E_1^{\ddagger}$	$\Delta E_2^{\ddagger}$	$\Delta E_3^{\ddagger}$	$\Delta E_h^{\ddagger}$
S	M06-L	9.9	0.8	4.6	13.7
	CCSD(T)	10.0	1.2	4.7	13.4
C	M06-L	10.9	2.1	5.0	13.7
	CCSD(T)	10.2	3.0	5.4	12.6
T = −80 °C		$\Delta G_1^{\ddagger}$	$\Delta G_2^{\ddagger}$	$\Delta G_3^{\ddagger}$	$\Delta G_h^{\ddagger}$
S	M06-L	9.5	0.4	2.9	12.0
	CCSD(T)	9.6	0.7	2.9	11.8
C	M06-L	11.2	1.7	4.0	13.5
	CCSD(T)	10.5	2.6	4.4	12.4
T = −50 °C		$\Delta G_1^{\ddagger}$	$\Delta G_2^{\ddagger}$	$\Delta G_3^{\ddagger}$	$\Delta G_h^{\ddagger}$
S	M06-L	9.6	0.4	2.8	12.0
	CCSD(T)	9.7	0.8	2.8	11.8
C	M06-L	11.4	1.7	4.0	13.7
	CCSD(T)	10.7	2.6	4.4	12.5
T = 25 °C		$\Delta G_1^{\ddagger}$	$\Delta G_2^{\ddagger}$	$\Delta G_3^{\ddagger}$	$\Delta G_h^{\ddagger}$
S	M06-L	9.9	0.5	2.6	12.0
	CCSD(T)	9.9	0.9	2.7	11.7
C	M06-L	11.9	1.9	4.1	14.1
	CCSD(T)	11.3	2.8	4.5	13.0

[a]The letters "S" and "C" denote simplified and complete structures of $ReH_5(PPh_3)_2$(pyridine) used for theoretical calculations, respectively. [b]The equivalent barrier of the high-temperature fluxional process is calculated by $\Delta E_h^{\ddagger} = \Delta E_1^{\ddagger} - \Delta E_2^{\ddagger} + \Delta E_3^{\ddagger}$ and $\Delta G_h^{\ddagger} = \Delta G_1^{\ddagger} - \Delta G_2^{\ddagger} + \Delta G_3^{\ddagger}$. [c]The level of theory for calculations can be found in the Computational Details section.

We employed both the complete rhenium polyhydride structure $ReH_5(PPh_3)_2$(pyridine) and its simplified structure $ReH_5(PH_3)_2$(pyridine) in our calculations. We denote $\Delta E_1^{\ddagger}$, $\Delta E_2^{\ddagger}$, and $\Delta E_3^{\ddagger}$ for the three electronic energy barriers of **LT** → **TS1**, **IM** → **TS1**, and **IM** → **TS2**, respectively. The free energy counterparts of $\Delta E^{\ddagger}$ are denoted as $\Delta G^{\ddagger}$.

As the measured energy barriers of the fluxional processes take the **LT** structure as the starting point,[43] the calculated

https://dx.doi.org/10.1021/acs.inorgchem.0c03418
Inorg. Chem. 2021, 60, 2492−2502

energy barrier for the low-temperature fluxional process is $\Delta E_1^{\ddagger}$ ($\Delta G_1^{\ddagger}$), while the energy barrier for the high-temperature fluxional process actually corresponds to the energy difference between **TS2** and **LT** denoted as $\Delta E_h^{\ddagger}$ ($\Delta G_h^{\ddagger}$).

Table 2 shows that the M06-L density functional and the DLPNO-CCSD(T) method give very similar energy barrier results with their differences all below 1 kcal/mol. Among four electronic energy barriers, the first three calculated with the complete rhenium polyhydride structure are all slightly larger than their counterparts calculated with the simplified structure. But in terms of free energy barriers, all four barriers calculated with the complete structure are higher. We calculated the free energy barriers at three different temperatures (−80, −50, and 25 °C) and found that $\Delta G_1^{\ddagger}$ values increase with the temperature. The $\Delta G_h^{\ddagger}$ values calculated with the complete structure follows the same trend but the $\Delta G_h^{\ddagger}$ calculated with the simplified structure stays almost the same given the temperature change.

In earlier work, the free energy barrier was measured at −80 °C to be 9.63 ± 0.25 kcal/mol and $\Delta G_h^{\ddagger}$ was measured at −50 °C to be 10.40 ± 0.25 kcal/mol.[44] We choose the free energy barriers calculated at the CCSD(T) level with both the simplified and complete structure at corresponding temperatures to be compared against the experimental values. With the simplified structural model, the two calculated barriers (i.e. $\Delta G_1^{\ddagger}$ and $\Delta G_h^{\ddagger}$) are 9.6 and 11.8 kcal/mol. The first value matches very well with the experiment while the second barrier is overestimated by more than 1 kcal/mol. With the complete structural model, two calculated barriers are consistently increased to 10.5 and 12.5 kcal/mol. The first calculated barrier is larger than the experimental barrier by 0.9 kcal/mol, which is still within the chemical accuracy. Although the error in the second calculated barrier is 2.1 kcal/mol, we need to note that the difference between the two measured barriers (i.e. $\Delta G_h^{\ddagger} - \Delta G_1^{\ddagger}$) is 0.77 ± 0.50 kcal/mol, while the calculated barrier difference is 2.0 kcal/mol. In summary, our calculated free energy barriers agree with the experimental values to a satisfactory extent even though we did not include multiple conformations of the bulky substituents (e.g. phenyl and pyridine rings) and the solvent environment into our calculations. On this basis, our calculations have demonstrated that the two types of three-arm turnstile rotation processes are the highly credible mechanisms which are responsible for the fluxionality in the rhenium polyhydride complex $ReH_5(PPh_3)_2$(pyridine).

The original report of the variable-temperature NMR spectra of $ReH_5(PPh_3)_2$(pyridine) by Crabtree and co-workers also describes the decoalescence of two meta protons on the pyridine ligand upon cooling, and the measured free energy barrier associated with this process was found to be the same as the barrier associated with the second coalescence event in the hydride region.[43] According to their analysis, the decoalescence of the pyridine resonance peaks can be attributed to two mechanisms: (1) the rotation of the Re−N bond by 180° and (2) the fluxionality in five hydrides leading to a pseudorotation of the whole molecule. While the second mechanism was preferred to explain the decoalescence for pyridine, it is still open to question and needs further justification. In order to gain some insight into this problem, we did further calculations on another simplified structure model $ReH_5(PPhH_2)_2$(pyridine) as well as on the complete structure (see section S5 in Supporting Information). According to our calculations at the M06-L(D3)/def2-TZVP level, the electronic energy barrier to rotate the pyridine ligand in $ReH_5(PPh_3)_2$(pyridine) is up to 13.0 kcal/mol which is very close to the barrier $\Delta E_h^{\ddagger}$ (13.7 kcal/mol) associated with the second coalescence event. Therefore, it is likely that the rotation of the Re−N bond takes place together with the pseudorotation process caused by hydride exchange in this rhenium polyhydride complex.

Influence from the Re−H···H−N/C Dihydrogen Bond. Many rhenium polyhydrides have been found to form dihydrogen bond interactions within themselves or in cocrystal structures.[37,38] In the work of Crabtree and co-workers, two additional rhenium polyhydride complexes $ReH_5(PPh_3)_2L$ were synthesized where the ligand L is either 2-(acetylamino)-pyridine or 4-(acetylamino)pyridine, which has the −NHAc group attached to the ortho or para position of pyridine, respectively.[44] They found that the −NHAc group in the ortho position of pyridine could lower the barrier for the low-temperature fluxional process (i.e. turnstile rotation in Figure 2) by more than 1 kcal/mol while the −NHAc group in the para position can only lower the same barrier by 0.3 kcal/mol. Besides, the barrier for the high-temperature fluxional process (i.e. pseudorotation in Figure 2) is marginally affected by the addition of the −NHAc group to either position. They ascribed the lowered barrier of the low-temperature fluxional process in $ReH_5(PPh_3)_2L$ (L = 2-(acetylamino)pyridine) to the presence of the intramolecular Re−H···H−N dihydrogen bond between the hydride and the −NHAc group based on the DFT calculations.

The dihydrogen bond between the transition-metal hydride (M−H) and a protic hydrogen moiety (H−X where X = N, O, C) is an important type of weak interaction which was first brought to the spotlight by Crabtree, Milstein, Morris, Shubina, and others in the 1990s.[36−38,61] As in this work, we have obtained a renewed perspective into the fluxional processes of $ReH_5(PPh_3)_2$(pyridine); it is therefore necessary to investigate in detail how the dihydrogen bond will influence the new mechanisms (i.e. lateral and basal three-arm turnstile rotations) and whether such influence is consistent with the experimental observations.

We first optimized the low-temperature structures of $ReH_5(PH_3)_2L$ (L = 2-(acetylamino)pyridine) at the M06-L(D3)/def2-SVP level in two conformations whose major difference lies in the 180° rotation of the Re−N bond (see Figure 5). Here, $ReH_5(PH_3)_2L$ is the simplified structure of $ReH_5(PPh_3)_2L$ by omitting the phenyl groups. Then, single-point energies of these two conformers were calculated at the M06-L(D3)/def2-TZVP and DLPNO-CCSD(T)/def2-TZVP levels. Both high-level quantum chemical methods give very similar energy results for these two conformers with the difference less than 0.2 kcal/mol. This means that the $ReH_5(PPh_3)_2L$ complex and its simplified structure $ReH_5(PH_3)_2L$ can adopt two conformations with equal population in the gas/liquid phase given its straightforward synthesis route.[39] Therefore, both conformations need to be considered when discussing the fluxional mechanisms of the $ReH_5(PPh_3)_2L$ complex. Noteworthy is that only conformer A was considered in the previous study by Crabtree and co-workers.[44]

As illustrated in Figure 5, the hydrogen atom on the amide nitrogen can have a close contact (i.e. dihydrogen bond) with the hydrides immediately underneath the −NHAc group in both conformers and these affected hydrides (especially in conformer A) participate in the lateral three-arm turnstile

https://dx.doi.org/10.1021/acs.inorgchem.0c03418
Inorg. Chem. 2021, 60, 2492−2502

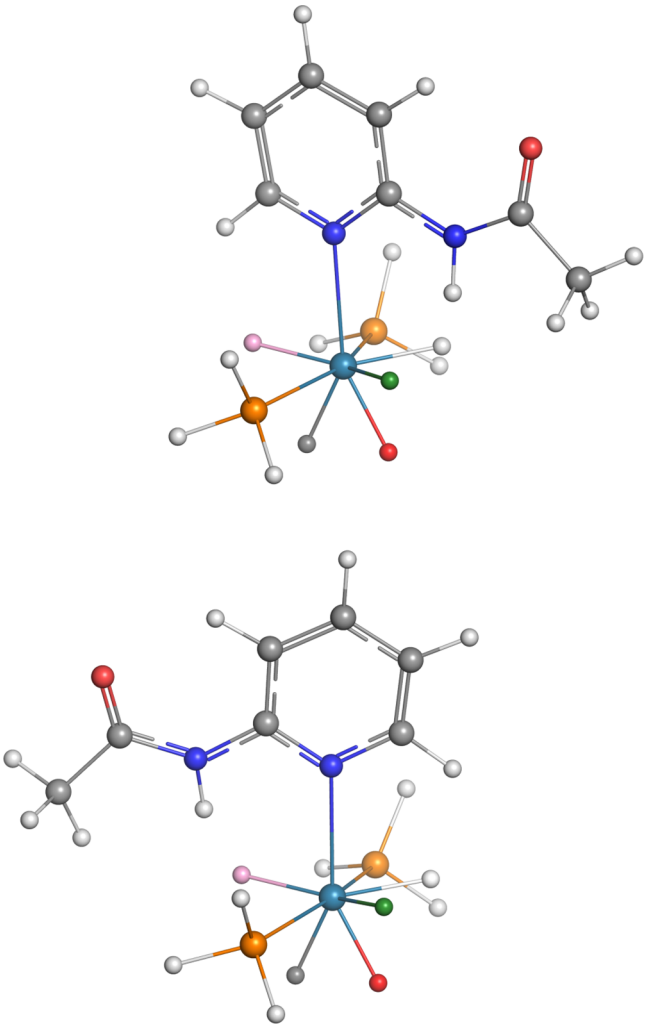

Figure 5. Low-temperature structures (**LT**) of $ReH_5(PH_3)_2L$ (L = 2-(acetylamino)pyridine) in conformations A (top) and B (bottom) optimized at the M06-L(D3)/def2-SVP level. The color scheme for five hydrides is consistent with that in Figures 1 and 4.

rotation process. However, the basal three-arm turnstile rotation occurring in the bottom is not directly affected by such close contact, although the pure electronic effect arising from the −NHAc group on pyridine could play a role in lowering the corresponding barrier height.[44] Therefore, we can just focus on the lateral turnstile mechanism in the following to disclose the role of the intramolecular dihydrogen bond on fluxionality.

We obtained the transition-state structures **TS1** for the lateral three-arm turnstile rotation mechanism in the two conformers of $ReH_5(PH_3)_2L$ (L = 2-(acetylamino)pyridine) in comparison to the **TS1** structure of $ReH_5(PH_3)_2$(pyridine) as shown in Figure 6. It is clearly illustrated in Figure 6d via the alignment of all three **TS1** structures that the added −NHAc group to pyridine does not change the transition-state geometry of the five hydrides.

Then, we calculated the energy barriers $\Delta E_1^{\ddagger}$ ($\Delta G_1^{\ddagger}$) for the lateral three-arm turnstile rotation mechanism of the two conformers of $ReH_5(PH_3)_2L$ (L = 2-(acetylamino)pyridine) at the M06-L(D3)/def2-TZVP and DLPNO-CCSD(T)/def2-TZVP levels (see Table 3). We found that two different levels

Table 3. Calculated Electronic and Free Energy Barriers (in kcal/mol) for the Lateral Three-Arm Turnstile Rotation of $ReH_5(PH_3)_2L$ (L = 2-(Acetylamino)pyridine)[a]

electronic	$\Delta E_1^{\ddagger}$		
Conformation	A	B	average
M06-L	7.3	10.7	9.0
CCSD(T)	6.4	10.2	8.3
T = −80 °C	$\Delta G_1^{\ddagger}$		
conformation	A	B	average
M06-L	6.6	9.6	8.1
CCSD(T)	5.7	9.2	7.4

[a]The level of theory for calculations can be found in the Computational Details section.

of theory render quite similar barrier results with differences all below 1 kcal/mol. Furthermore, both the electronic and free energy barriers in the conformer B are larger than those in the conformer A by more than 3 kcal/mol. By comparing these calculated barriers of $ReH_5(PH_3)_2L$ with the calculated barriers for the same lateral turnstile mechanism of $ReH_5(PH_3)_2$(pyridine) as collected in Table 2, conformer B of $ReH_5(PH_3)_2L$ has slightly higher electronic energy barriers (10.7/10.2 vs 9.9/10.0 kcal/mol) while its free energy barriers

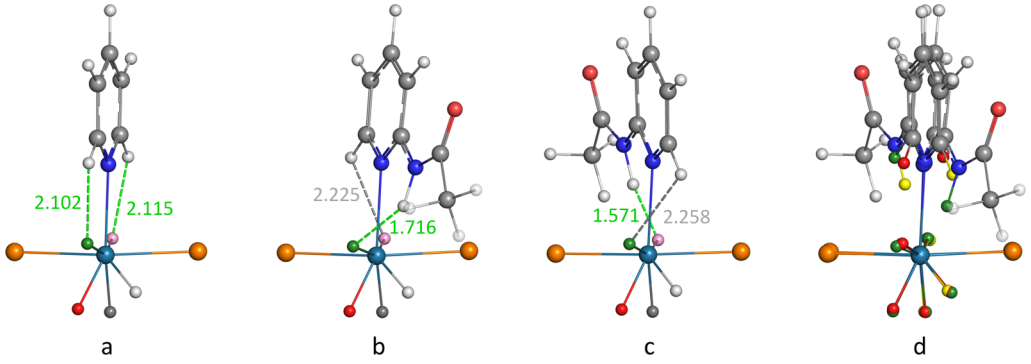

Figure 6. (a) **TS1** structure of $ReH_5(PH_3)_2$(pyridine). (b,c) **TS1** structures of $ReH_5(PH_3)_2L$ (L = 2-(acetylamino)pyridine) in conformations A and B, respectively. (d) Alignment of all preceding three **TS1** structures with seven hydrogen atoms colored in red, green, and yellow, respectively. All three **TS1** structures were optimized at the M06-L(D3)/def2-SVP level. The color scheme for five hydrides in (a) through (c) is consistent with that in Figures 1 and 4. The Re−H···H−N/C dihydrogen bond is shown as the dashed line labeled with the distance in Angstrom. The dihydrogen interactions colored in green and gray represent the presence and absence of the bond critical point (BCP), respectively.

https://dx.doi.org/10.1021/acs.inorgchem.0c03418
Inorg. Chem. 2021, 60, 2492−2502

are equivalent to or marginally smaller than the $ReH_5(PH_3)_2$(pyridine) case (9.6/9.2 vs 9.5/9.6 kcal/mol). Besides, the electronic and free energy barriers of conformer A of $ReH_5(PH_3)_2L$ are significantly smaller than the corresponding barriers of $ReH_5(PH_3)_2$(pyridine). This means that conformer B of $ReH_5(PPh_3)_2L$ in the liquid NMR sample (with CD_2Cl_2 solvent) would exhibit very similar behavior as $ReH_5(PPh_3)_2$(pyridine) during the first coalescence event upon heating in terms of the temperature range. Conformer A of $ReH_5(PPh_3)_2L$ in the same liquid NMR sample is expected to show the earlier first coalescence event at a lower temperature than conformer B because its corresponding energy barrier is around 3 kcal/mol lower. Therefore, the presence of two conformations in $ReH_5(PPh_3)_2L$ in the liquid NMR sample complicates the variable-temperature NMR spectra and leads to a larger error (than 0.25 kcal/mol) in the measured energy barrier for the low-temperature fluxional process. Assuming that the two conformers of $ReH_5(PPh_3)_2L$ coexist in the CD_2Cl_2 solvent with about the same population due to very close electronic energies for the two conformers of the simplified structure $ReH_5(PH_3)_2L$, we took the average value of the two corresponding energy barriers as the measurable barrier (see Table 3). If we focus on the simplified structures including $ReH_5(PH_3)_2$(pyridine) and $ReH_5(PH_3)_2L$, the corresponding calculated free energy barriers $\Delta G_1^{\ddagger}$ at −80 °C are 9.5/9.6 and 8.1/7.4 kcal/mol, respectively. The experimentally measured $\Delta G_1^{\ddagger}$ values for $ReH_5(PPh_3)_2$(pyridine) and $ReH_5(PPh_3)_2L$ are 9.63 ± 0.25 and 8.58 ± 0.25 kcal/mol, respectively.[44] Therefore, the addition of the −NHAc group to the ortho position of pyridine lowers $\Delta G_1^{\ddagger}$ by 1.1 ± 0.5 kcal/mol in experiments while our calculation based on the simplified structural model indicates the lowered barrier by ca. 1.8 kcal/mol which is quantitatively consistent with the experimental observation.

However, the important question that remains to be answered is why the energy barrier for the lateral turnstile rotation of the conformer A of $ReH_5(PH_3)_2L$ (L = 2-(acetylamino)pyridine) is significantly lowered compared to $ReH_5(PH_3)_2$(pyridine) while the same barrier of the conformer B is almost unchanged. Figure 6 shows the **TS1** structures for $ReH_5(PH_3)_2$(pyridine) and the two conformers of $ReH_5(PH_3)_2L$, where the triad of hydrides participating in the lateral turnstile rotation is colored in green, red, and white. There exist two Re−H···H−C dihydrogen bonds in the **TS1** structure of $ReH_5(PH_3)_2$(pyridine), and one of them involves the green hydride with the bond length of 2.1 Å. In the case of conformer B of $ReH_5(PH_3)_2L$ (see Figure 6c), there exists one Re−H···H−N dihydrogen bond with the pink hydride and one Re−H···H−C dihydrogen bond with the green hydride in the length of 2.3 Å. The conformer A of $ReH_5(PH_3)_2L$ (see Figure 6b) also has two dihydrogen bonds but one of them is a Re−H···H−N interaction with the green hydride in the length of 1.7 Å. As it is easy to understand that a Re−H···H−N dihydrogen bond is generally stronger than the Re−H···H−C counterpart,[38] the green hydride in the conformer A of $ReH_5(PH_3)_2L$ is connected with the strongest dihydrogen bond among all three **TS1** structures. Therefore, the transition state structure in conformer A is best stabilized by the dihydrogen bond, and the corresponding energy barrier is significantly reduced.

CONCLUSIONS

In this work, we have employed the state-of-the-art quantum chemical calculations and identified two plausible fluxional mechanisms for the rhenium polyhydride complex $ReH_5(PPh_3)_2$(pyridine) including the lateral and basal three-arm turnstile rotations to explain the two successive coalescence events in the hydride region of the variable-temperature NMR spectra. In comparison with earlier suggested mechanisms (see Figure 2) for the same polyhydride complex,[43] the lateral three-arm turnstile mechanism proposed in this work can be considered as a revised version of Crabtree's turnstile mechanism[44] while the basal three-arm turnstile mechanism proposed in this work is new and does not lead to Crabtree's pseudorotation for the low-temperature structure by itself. According to the new fluxional mechanisms, the pseudorotation for the low-temperature structure requires two lateral three-arm turnstile processes and one basal three-arm turnstile process in between, which is significantly different from Crabtree's one-step pseudorotation mechanism. Furthermore, we have also studied the influence from the intramolecular dihydrogen bond arising from the −NHAc group on the ortho position of the pyridine ligand to further verify the new fluxional mechanisms. Therefore, our work provides renewed insights into the mechanistic details of the fluxionality in the rhenium polyhydride complex $ReH_5(PPh_3)_2$(pyridine).

On this basis, we will further examine the rotational flexibility of the pyridine ligand[27] and the hydrogen exchange with a water molecule in other rhenium polyhydride structures similar to $ReH_5(PPh_3)_2$(pyridine).[28] In addition, the observation of three separate coalescences in the hydride NMR peaks[62] and the occurrence of coalescence in the phosphorus resonances[29] are part of the unsolved fluxionality puzzles in octacoordinate rhenium polyhydrides. Computational studies of these problems will help us to depict a more complete picture of fluxionality in rhenium polyhydrides.

We believe that the lateral and basal three-arm turnstile mechanisms proposed in this work may exist not only in the rhenium polyhydride complexes[29,40−42,62−65] which are structurally similar to $ReH_5(PPh_3)_2$(pyridine) but also in the other metal polyhydride complexes of the high coordination number.[30,45,66] This work fills a gap in the fluxionality of octacoordinate compounds[24,67,68] which are less explored compared with the fluxionality in the compounds with a lower coordination number, and more work is planned in this direction.

ASSOCIATED CONTENT

Supporting Information

The Supporting Information is available free of charge at https://pubs.acs.org/doi/10.1021/acs.inorgchem.0c03418.

Cartesian coordinates of the stationary-point structures for rhenium polyhydride systems discussed in this work and the comparison in the transition-state geometries optimized by M06-L and B3LYP functionals (PDF)

AUTHOR INFORMATION

Corresponding Author

Elfi Kraka − *Department of Chemistry, Southern Methodist University, Dallas, Texas 75275-0314, United States;* orcid.org/0000-0002-9658-5626; Email: ekraka@gmail.com

https://dx.doi.org/10.1021/acs.inorgchem.0c03418
Inorg. Chem. 2021, 60, 2492−2502

Authors

Yunwen Tao − *Department of Chemistry, Southern Methodist University, Dallas, Texas 75275-0314, United States*

Wenli Zou − *Institute of Modern Physics, Northwest University, and Shaanxi Key Laboratory for Theoretical Physics Frontiers, Xi'an, Shaanxi 710127, P. R. China;* orcid.org/0000-0002-0747-2428

Geng-Geng Luo − *Key Laboratory of Environmental Friendly Function Materials, Ministry of Education, and College of Materials Science and Engineering, Huaqiao University, Xiamen, Fujian 361021, P. R. China*

Complete contact information is available at: https://pubs.acs.org/10.1021/acs.inorgchem.0c03418

Notes

The authors declare no competing financial interest.

■ ACKNOWLEDGMENTS

This work was financially supported by the National Science Foundation (Grant CHE 1464906). We thank SMU for providing generous computational resources. W.Z. also acknowledges the financial support by the National Natural Science Foundation of China (Grant no. 21673175) and the Double First-Class University Construction Project of Northwest University. Y.T. thanks Linyao Zhang and Yue Qiu for helpful discussions.

■ REFERENCES

(1) Moss, G. P. Basic Terminology of Stereochemistry (IUPAC Recommendations 1996). *Pure Appl. Chem.* **1996**, *68*, 2193−2222. polytopal rearrangement on page 2213; pseudorotation on page 2215

(2) Muetterties, E. L. Topological Representation of Stereoisomerism. I. Polytopal Rearrangements. *J. Am. Chem. Soc.* **1969**, *91*, 1636−1643.

(3) Lai, J.-C.; Jia, X.-Y.; Wang, D.-P.; Deng, Y.-B.; Zheng, P.; Li, C.-H.; Zuo, J.-L.; Bao, Z. Thermodynamically Stable Whilst Kinetically Labile Coordination Bonds Lead to Strong and Tough Self-Healing Polymers. *Nat. Commun.* **2019**, *10*. DOI: 10.1038/s41467-019-09130-z

(4) Berry, R. S. Correlation of Rates of Intramolecular Tunneling Processes, with Application to Some Group V Compounds. *J. Chem. Phys.* **1960**, *32*, 933−938.

(5) Berry, R. S. Time-Dependent Measurements and Molecular Structure: Ozone. *Rev. Mod. Phys.* **1960**, *32*, 447−454.

(6) Taha, A. N.; True, N. S.; LeMaster, C. B.; LeMaster, C. L.; Neugebauer-Crawford, S. M. Gas-Phase Nuclear Magnetic Resonance Study of Berry Pseudorotation of SF_4. Comparison of Experimental and Calculated Kinetic Parameters and Falloff Kinetics. *J. Phys. Chem. A* **2000**, *104*, 3341−3348.

(7) Minyaev, R. M.; Wales, D. J. Transition Vector Symmetry and the Internal Pseudo-Rotation and Inversion Paths of CIF4 +. *J. Chem. Soc., Faraday Trans.* **1994**, *90*, 1831−1837.

(8) Muetterties, E. L. Topological Representation of Stereoisomerism. II. The Five-Atom Family. *J. Am. Chem. Soc.* **1969**, *91*, 4115−4122.

(9) Rzepa, H. S.; Cass, M. E. A Computational Study of the Nondissociative Mechanisms that Interchange Apical and Equatorial Atoms in Square Pyramidal Molecules. *Inorg. Chem.* **2006**, *45*, 3958−3963.

(10) Bailar, J. C., Jr. Some Problems in the Stereochemistry of Coordination Compounds: Introductory Lecture. *J. Inorg. Nucl. Chem.* **1958**, *8*, 165−175.

(11) Ray, P.; Dutt, N. Kinetics and Mechanism of Racemization of Optically Active Cobaltic Trisbiguanide Complex. *J. Indian Chem. Soc.* **1943**, *20*, 81−92.

(12) Adams, W. J.; Thompson, H. B.; Bartell, L. S. Structure, Pseudorotation, and Vibrational Mode Coupling in IF_7: An Electron Diffraction Study. *J. Chem. Phys.* **1970**, *53*, 4040−4046.

(13) Nikitin, K.; O'Gara, R. Mechanisms and Beyond: Elucidation of Fluxional Dynamics by Exchange NMR Spectroscopy. *Eur. J. Chem.* **2019**, *25*, 4551−4589.

(14) Sandström, J. *Dynamic NMR Spectroscopy*; Academic Press, 1982.

(15) Bryant, R. G. The NMR Time Scale. *J. Chem. Educ.* **1983**, *60*, 933.

(16) Crabtree, R. *The Organometallic Chemistry of the Transition Metals*; Wiley: Hoboken, New Jersey, 2014.

(17) Harvey, J. N.; Himo, F.; Maseras, F.; Perrin, L. Scope and Challenge of Computational Methods for Studying Mechanism and Reactivity in Homogeneous Catalysis. *ACS Catal.* **2019**, *9*, 6803−6813.

(18) Mauksch, M.; Schleyer, P. v. R. Effective Monkey Saddle Points and Berry and Lever Mechanisms in the Topomerization of SF_4 and Related Tetracoordinated AX_4 Species. *Inorg. Chem.* **2001**, *40*, 1756−1769.

(19) Cass, M. E.; Hii, K. K.; Rzepa, H. S. Mechanisms That Interchange Axial and Equatorial Atoms in Fluxional Processes: Illustration of the Berry Pseudorotation, the Turnstile, and the Lever Mechanisms via Animation of Transition State Normal Vibrational Modes. *J. Chem. Educ.* **2006**, *83*, 336.

(20) Rzepa, H. S.; Cass, M. E. Search of the Bailar and Rây-Dutt Twist Mechanisms That Racemize Chiral Trischelates: A Computational Study of Sc^{III}, Ti^{IV}, Co^{III}, Zn^{II}, Ga^{III}, and Ge^{IV} Complexes of a Ligand Analogue of Acetylacetonate. *Inorg. Chem.* **2007**, *46*, 8024−8031.

(21) Couzijn, E. P. A.; Slootweg, J. C.; Ehlers, A. W.; Lammertsma, K. Stereomutation of Pentavalent Compounds: Validating the Berry Pseudorotation, Redressing Ugi's Turnstile Rotation, and Revealing the Two- and Three-Arm Turnstiles. *J. Am. Chem. Soc.* **2010**, *132*, 18127−18140.

(22) Asatryan, R.; Ruckenstein, E.; Hachmann, J. Revisiting the Polytopal Rearrangements in Penta-Coordinate d^7-Metallocomplexes: Modified Berry Pseudorotation, Octahedral Switch, and Butterfly Isomerization. *Chem. Sci.* **2017**, *8*, 5512−5525.

(23) Zou, W.; Tao, Y.; Kraka, E. Describing Polytopal Rearrangements of Fluxional Molecules with Curvilinear Coordinates Derived from Normal Vibrational Modes: A Conceptual Extension of Cremer-Pople Puckering Coordinates. *J. Chem. Theory Comput.* **2020**, *16*, 3162−3193.

(24) Burdett, J. K.; Hoffmann, R.; Fay, R. C. Eight-Coordination. *Inorg. Chem.* **1978**, *17*, 2553−2568.

(25) King, R. B. Chemical Applications of Topology and Group Theory. 20. Eight-Vertex Polyhedra and Their Rearrangements. *Inorg. Chem.* **1986**, *25*, 506−510.

(26) Weir, J. R.; Fay, R. C. Stereochemistry and Metal-Centered Rearrangements of Eight-Coordinate Niobium(V) and Tantalum(V) Dithiocarbamates and Monothiocarbamates. *Inorg. Chem.* **1986**, *25*, 2969−2976.

(27) Jimenez, Y.; Strepka, A. M.; Borgohain, M. D.; Hinojosa, P. A.; Moehring, G. A. Ortho-Metalation, Rotational Isomerization, and Hydride-Hydride Coupling at Rhenium (V) Polyhydride Complexes Stabilized by Aromatic Amine Ligands. *Inorg. Chim. Acta* **2009**, *362*, 3259−3266.

(28) Streisel, D. J.; Petrou, A. L.; Scorzelli, A. G.; Macalush, B. E.; Siebert, H. M.; Torres, G. S.; Joswick, C. M.; Moehring, G. A. Fluxionality, Substitution, and Hydrogen Exchange at Eight-Coordinate Rhenium(V) Polyhydride Centers. *Inorg. Chim. Acta* **2019**, *496*, 119028.

(29) Scorzelli, A. G.; Macalush, B. E.; Naik, D. V.; Moehring, G. A. Comparative Study of Fluxional Processes at Two Different Classes of Eight-Coordinate Rhenium(V) Polyhydride Complexes. *Inorg. Chim. Acta* **2021**, *516*, 120120.

(30) Hlatky, G. G.; Crabtree, R. H. Transition-Metal Polyhydride Complexes. *Coord. Chem. Rev.* **1985**, *65*, 1−48.

(31) O'Connor, J. M. In *Comprehensive Organometallic Chemistry II*; Abel, E. W., Stone, F. G. A., Wilkinson, G., Eds.; Elsevier, 1995; Vol. 6; pp 180−188.
(32) Takaya, H.; Ito, M.; Murahashi, S.-I. Rhenium-Catalyzed Addition of Carbonyl Compounds to the Carbon-Nitrogen Triple Bonds of Nitriles: α-C-H Activation of Carbonyl Compounds. *J. Am. Chem. Soc.* **2009**, *131*, 10824−10825.
(33) Schleker, P. P. M.; Honeker, R.; Klankermayer, J.; Leitner, W. Catalytic Dehydrogenative Amide and Ester Formation with Rhenium-Triphos Complexes. *ChemCatChem* **2013**, *5*, 1762−1764.
(34) Jin, H.; Xie, J.; Pan, C.; Zhu, Z.; Cheng, Y.; Zhu, C. Rhenium-Catalyzed Acceptorless Dehydrogenative Coupling via Dual Activation of Alcohols and Carbonyl Compounds. *ACS Catal.* **2013**, *3*, 2195−2198.
(35) Jin, H.; Zhu, Z.; Jin, N.; Xie, J.; Cheng, Y.; Zhu, C. CO-Enabled Rhenium Hydride Catalyst for Directed C(sp^2)−H Bond Alkylation with Olefins. *Org. Chem. Front.* **2015**, *2*, 378−382.
(36) Wessel, J.; Lee, J. C.; Peris, E.; Yap, G. P. A.; Fortin, J. B.; Ricci, J. S.; Sini, G.; Albinati, A.; Koetzle, T. F.; Eisenstein, O.; Rheingold, A. L.; Crabtree, R. H. An Unconventional Intermolecular Three-Center N−H···H2Re Hydrogen Bond in Crystalline [ReH5(PPh3)3]·indole·C6H6. *Angew. Chem., Int. Ed.* **1995**, *34*, 2507−2509.
(37) Crabtree, R. H.; Siegbahn, P. E. M.; Eisenstein, O.; Rheingold, A. L.; Koetzle, T. F. A New Intermolecular Interaction: Unconventional Hydrogen Bonds with Element−Hydride Bonds as Proton Acceptor. *Acc. Chem. Res.* **1996**, *29*, 348−354.
(38) Belkova, N. V.; Epstein, L. M.; Filippov, O. A.; Shubina, E. S. Hydrogen and Dihydrogen Bonds in the Reactions of Metal Hydrides. *Chem. Rev.* **2016**, *116*, 8545−8587.
(39) Chatt, J.; Coffey, R. S. Hydrido-Complexes of Rhenium-Containing Tertiary Phosphines. *J. Chem. Soc. A* **1969**, 1963.
(40) Albinati, A.; Bakhmutov, V. I.; Belkova, N. V.; Bianchini, C.; Rios, I. d. l.; Epstein, L.; Gutsul, E. I.; Marvelli, L.; Peruzzini, M.; Rossi, R.; Shubina, E.; Vorontsov, E. V.; Zanobini, F. Synthesis, Characterization, and Interconversion of the Rhenium Polyhydrides $[ReH_3(\eta^4\text{-}NP_3)]$ and $[ReH_4(\eta^4\text{-}NP_3)]^+$ {NP_3 = tris[2-(diphenylphosphanyl)ethyl]amine}. *Eur. J. Inorg. Chem.* **2002**, 1530−1539.
(41) Bolaño, S.; Bravo, J.; García-Fontán, S. Mono- and Dinuclear Rhenium Polyhydride Complexes Bearing the Chelating Ligand 1,2-Bis(dicyclohexylphosphanyloxy)ethane. *Eur. J. Inorg. Chem.* **2004**, 4812−4819.
(42) Bolaño, S.; Gonsalvi, L.; Barbaro, P.; Albinati, A.; Rizzato, S.; Gutsul, E.; Belkova, N.; Epstein, L.; Shubina, E.; Peruzzini, M. Synthesis, Characterization, Protonation Studies and X-Ray Crystal Structure of $ReH_5(PPh_3)_2$(PTA) (PTA=1,3,5-triaza-7-phosphaadamantane). *J. Organomet. Chem.* **2006**, *691*, 629−637.
(43) Lee, J. C.; Yao, W.; Crabtree, R. H.; Rüegger, H. Fluxionality in [ReH5(PPh3)2(pyridine)]. *Inorg. Chem.* **1996**, *35*, 695−699.
(44) Bosque, R.; Maseras, F.; Eisenstein, O.; Patel, B. P.; Yao, W.; Crabtree, R. H. Site Preference Energetics, Fluxionality, and Intramolecular M-H···H-N Hydrogen Bonding in a Dodecahedral Transition Metal Polyhydride. *Inorg. Chem.* **1997**, *36*, 5505−5511.
(45) Maseras, F.; Lledós, A.; Clot, E.; Eisenstein, O. Transition Metal Polyhydrides: From Qualitative Ideas to Reliable Computational Studies. *Chem. Rev.* **2000**, *100*, 601−636.
(46) Zhao, Y.; Truhlar, D. G. A New Local Density Functional for Main-Group Thermochemistry, Transition Metal Bonding, Thermochemical Kinetics, and Noncovalent Interactions. *J. Chem. Phys.* **2006**, *125*, 194101.
(47) Weigend, F.; Ahlrichs, R. Balanced Basis Sets of Split Valence, Triple Zeta Valence and Quadruple Zeta Valence Quality for H to Rn: Design and Assessment of Accuracy. *Phys. Chem. Chem. Phys.* **2005**, *7*, 3297.
(48) Weigend, F. Accurate Coulomb-Fitting Basis Sets for H to Rn. *Phys. Chem. Chem. Phys.* **2006**, *8*, 1057.
(49) Grimme, S.; Antony, J.; Ehrlich, S.; Krieg, H. A Consistent and Accurate *ab initio* Parametrization of Density Functional Dispersion Correction (DFT-D) for the 94 Elements H-Pu. *J. Chem. Phys.* **2010**, *132*, 154104.
(50) Hratchian, H. P.; Kraka, E. Improved Predictor-Corrector Integrators For Evaluating Reaction Path Curvature. *J. Chem. Theory Comput.* **2013**, *9*, 1481−1488.
(51) Tomasi, J.; Mennucci, B.; Cammi, R. Quantum Mechanical Continuum Solvation Models. *Chem. Rev.* **2005**, *105*, 2999−3094.
(52) Liakos, D. G.; Guo, Y.; Neese, F. Comprehensive Benchmark Results for the Domain Based Local Pair Natural Orbital Coupled Cluster Method (DLPNO-CCSD(T)) for Closed- and Open-Shell Systems. *J. Phys. Chem. A* **2019**, *124*, 90−100.
(53) Hellweg, A.; Hättig, C.; Höfener, S.; Klopper, W. Optimized Accurate Auxiliary Basis Sets for RI-MP2 and RI-CC2 Calculations for the Atoms Rb to Rn. *Theor. Chem. Acc.* **2007**, *117*, 587−597.
(54) Neese, F. Software update: the ORCA program system, version 4.0. *Mol. Sci.* **2018**, *8*, No. e1327.
(55) Frisch, M. J.; Trucks, G. W.; Schlegel, H. B.; Scuseria, G. E.; Robb, M. A.; Cheeseman, J. R.; Scalmani, G.; Barone, V.; Petersson, G. A.; Nakatsuji, H.; Li, X.; Caricato, M.; Marenich, A. V.; Bloino, J.; Janesko, B. G.; Gomperts, R.; Mennucci, B.; Hratchian, H. P.; Ortiz, J. V.; Izmaylov, A. F.; Sonnenberg, J. L.; Williams-Young, D.; Ding, F.; Lipparini, F.; Egidi, F.; Goings, J.; Peng, B.; Petrone, A.; Henderson, T.; Ranasinghe, D.; Zakrzewski, V. G.; Gao, J.; Rega, N.; Zheng, G.; Liang, W.; Hada, M.; Ehara, M.; Toyota, K.; Fukuda, R.; Hasegawa, J.; Ishida, M.; Nakajima, T.; Honda, Y.; Kitao, O.; Nakai, H.; Vreven, T.; Throssell, K.; Montgomery, J. A., Jr.; Peralta, J. E.; Ogliaro, F.; Bearpark, M. J.; Heyd, J. J.; Brothers, E. N.; Kudin, K. N.; Staroverov, V. N.; Keith, T. A.; Kobayashi, R.; Normand, J.; Raghavachari, K.; Rendell, A. P.; Burant, J. C.; Iyengar, S. S.; Tomasi, J.; Cossi, M.; Millam, J. M.; Klene, M.; Adamo, C.; Cammi, R.; Ochterski, J. W.; Martin, R. L.; Morokuma, K.; Farkas, O.; Foresman, J. B.; Fox, D. J. *Gaussian 16*, Revision B.01.; Gaussian Inc: Wallingford CT, 2016.
(56) Bax, A.; Davis, D. G. Practical Aspects of Two-Dimensional Transverse NOE Spectroscopy. *J. Magn. Reson.* **1985**, *63*, 207−213.
(57) Oguadinma, P.; Bilodeau, F.; LaPlante, S. R. NMR Strategies to Support Medicinal Chemistry Workflows for Primary Structure Determination. *Bioorg. Med. Chem. Lett.* **2017**, *27*, 242−247.
(58) Stephens, P. J.; Devlin, F. J.; Chabalowski, C. F.; Frisch, M. J. Ab Initio Calculation of Vibrational Absorption and Circular Dichroism Spectra Using Density Functional Force Fields. *J. Phys. Chem.* **1994**, *98*, 11623−11627.
(59) Hammond, G. S. A Correlation of Reaction Rates. *J. Am. Chem. Soc.* **1955**, *77*, 334−338.
(60) Leffler, J. E. Parameters for the Description of Transition States. *Science* **1953**, *117*, 340−341.
(61) Stevens, R. C.; Bau, R.; Milstein, D.; Blum, O.; Koetzle, T. F. Concept of the H(δ +)··· H(δ−) Interaction. A Low-Temperature Neutron Diffraction Study of cis-$[IrH(OH)(PMe_3)_4]PF_6$. *J. Chem. Soc., Dalton Trans.* **1990**, 1429−1432.
(62) Ginsberg, A. P.; Abrahams, S. C.; Jamieson, P. B. Nonrigid Stereochemistry in Eight-Coordinate Pentahydridorhenium Complexes. *J. Am. Chem. Soc.* **1973**, *95*, 4751−4752.
(63) Luo, X. L.; Crabtree, R. H. Synthesis and Structural Studies of Some New Rhenium Phosphine Heptahydride Complexes. Evidence for Classical Structures in Solution. *J. Am. Chem. Soc.* **1990**, *112*, 4813−4821.
(64) Leeaphon, M.; Ondracek, A. L.; Thomas, R. J.; Fanwick, P. E.; Walton, R. A. Reactions of Rhenium Polyhydrides with Internal and Terminal Alkynes as a Route to a New Class of Hydrido-Alkylidyne Complexes. *J. Am. Chem. Soc.* **1995**, *117*, 9715−9724.
(65) Bolaño, S.; Bravo, J.; García-Fontán, S.; Castro, J. Rhenium Pentahydride Complexes: Characterisation and Protonation Reactions. Crystal Structure of $ReH_5L^1L^2$ (L^1=$Ph_2PO(CH_2)_2OPPh_2$; L^2=$P(OCH_3)_3$, $P(OCH_2CH_3)_3$). *J. Organomet. Chem.* **2003**, *667*, 103−111.
(66) Gusev, D. G.; Berke, H. Hydride Fluxionality in Transition Metal Complexes: An Approach to the Understanding of Mechanistic Features and Structural Diversities. *Chem. Ber.* **1996**, *129*, 1143−1155.

https://dx.doi.org/10.1021/acs.inorgchem.0c03418
Inorg. Chem. 2021, 60, 2492−2502

(67) Muetterties, E. L. Stereochemical Lability of Eight-Coordinate Complexes. *Inorg. Chem.* **1973**, *12*, 1963−1966.
(68) Casanova, D.; Llunell, M.; Alemany, P.; Alvarez, S. The Rich Stereochemistry of Eight-Vertex Polyhedra: A Continuous Shape Measures Study. *Chem. Eur J.* **2005**, *11*, 1479−1494.

https://dx.doi.org/10.1021/acs.inorgchem.0c03418
Inorg. Chem. 2021, 60, 2492−2502